



Full Length Article

Parameters optimization for synthesis of Al-doped ZnO nanoparticles by laser ablation in water

Nikša Krstulović^{a,*}, Krešimir Salamon^{a,c}, Ognjen Budimlija^a, Janez Kovač^b, Jasna Dasović^c, Polona Umek^b, Ivana Čapan^c^a Institute of Physics, Bijenička cesta 46, 10 000 Zagreb, Croatia^b Jožef Stefan Institute, Jamova cesta 39, 1 000 Ljubljana, Slovenia^c Ruđer Bošković Institute, Bijenička cesta 54, 10 000 Zagreb, Croatia

ARTICLE INFO

Article history:

Received 12 October 2017

Revised 25 January 2018

Accepted 30 January 2018

Available online 1 February 2018

Keywords:

ZnO

Nanoparticles

Al-doped ZnO nanoparticles

Laser ablation in liquids

Laser synthesis of ZnO nanoparticles

Colloids

ABSTRACT

Al-doped ZnO crystalline colloidal nanoparticles were synthesized by a laser ablation of ZnO:Al₂O₃ in MilliQ water. Experiments were performed systematically by changing the number of applied laser pulses and laser output energy with the aim to affect the nanoparticle size, composition (Al/Zn ratio) and characteristics (band-gap, crystallinity). Distinctly, set of nanoparticle syntheses was performed in deionized water for comparison. SEM investigation of colloidal nanoparticles revealed that the formed nanoparticles are 30 nm thick discs with average diameters ranging from 450 to 510 nm. It was found that craters in the target formed during the laser ablation influence the size of synthesized colloidal nanoparticles. This is explained by efficient nanoparticle growth through diffusion process which take place in spatially restricted volume of the target crater. When laser ablation takes place in deionized water the synthesized nanoparticles have a mesh-like structure with sparse concentration of disc-like nanoparticles. Al/Zn ratio and band-gap energy of nanoparticles are highly influenced by the number and output energy of applied laser pulses. In addition, the procedure how to calculate the concentration of colloidal nanoparticles synthesized by laser ablation in liquids is proposed. The Al-doped ZnO colloidal nanoparticles properties were obtained using different techniques like scanning electron microscopy, optical microscopy, energy-dispersive X-ray spectroscopy, grazing-incidence X-ray diffraction, photoabsorption, photoluminescence and X-ray photoelectron spectroscopy.

© 2018 Elsevier B.V. All rights reserved.

1. Introduction

Here we introduce a synthesis of Al-doped ZnO nanoparticles in liquids by laser ablation in liquids (LAL) technique. This technique is based on the process of pulsed laser ablation of metallic target immersed in a liquid [1–3]. There are many advantages of this technique over standard ones but they are still not fully exploited. In particular, LAL is a very simple, fast, efficient and environmentally-friendly technique for convenient synthesis of nanoparticles colloidal solutions of wide range of materials and of wide range of nanoparticle types [4,5]. It is known as ‘green synthesis’ technique as no chemicals are required for synthesis processes [6] making this technique residues- and byproducts-free. This technique is not limited by a choice of materials as any metal target can be ablated. Moreover, not only metallic but other material (composites, isolators, conductive materials, semiconductors,

organic materials, ceramics, catalytic, hybrid and magnetic or paramagnetic materials) can be used for the colloidal nanoparticle synthesis by LAL [7–18] while synthesis can be done in wide variety of liquids for tailoring the nanoparticles properties [19]. In addition, laser pulses can additionally generate, de-agglomerate, fragmentate, re-shape and reduce the size of the initial nanoparticle colloidal solution either in a form of secondary laser interaction (post-irradiation) [20–23] or double-pulse LAL [24–26] by the processes described in [27].

ZnO is one of the most interesting materials due to the wide variety of applications in material science, environmental monitoring, energy storage and bio-medical sciences. ZnO is used for development of LED sources [28], photodetectors [29], gas sensors [30], as optical waveguide material [31] and as laser source [32,33]. Another promising applications are found among protective coatings such as an energy saving on windows or corrosion resistant on steel coatings [34] or as UV protective coatings for health care [35] or general purposes [36]. In addition, protective coatings are needed for the transparent thin-film transistors, where

* Corresponding author.

E-mail address: niksak@ifs.hr (N. Krstulović).

ZnO-based transistors are insensitive to visible light. Generally, ZnO is a promising material for optoelectronic devices [37] due to a confinement effects, but its low conductivity limits the spectra of applications. One way how to overcome this problem is n-type or p-type doping [38,39] while n-type doping is still a challenge due to known difficulties [40,41].

Physical properties of nanoparticles may additionally be improved by nanoparticles doping with various doping agents. By doping the nanoparticles may shift the photoluminescence emission to a specific range or have simultaneous emission from different parts of spectral range [42,43]. The possibility to change the emission peak and intensity is very important for bioimaging but also for development of luminescent phosphor-based lighting devices due to prolonged emission after the excitation is switched-off [44,45]. The other application is in photonics due to achieved up-conversion effect [46,47]. However, fabrication of doped nanoparticles is an issue as high-temperature chemical reactions to synthesize the nanoparticles are often required which, from one side, ensure high-quality nanoparticles, but from the other hand, it induces segregation of dopants on the particle surface [48,49]. Here we show that crystalline Al-doped ZnO nanoparticles may be synthesized in one-step by LAL of Al-doped ZnO target immersed in water. ZnO material is non-toxic and low-cost and its transport properties may be tuned by doping [50]. It was found that doping of ZnO nanoparticles with Al may enhance the sensitivity and the selectivity for developments of gas sensors [51] and thermoelectric properties (several-fold decrease of the thermal conductivity) [52]. Doping of ZnO with Al have a wide commercial use and broad spectrum of applications. Regarding the ideal doping level it was found that 2 wt.% of Al₂O₃ is an optimized balance between its electrical (low resistivity) [53] and optical (good transparency) [54] properties.

Beside ZnO thin films and related nanostructures [55,56], the synthesis of ZnO nanoparticles by laser ablation in liquids (LAL) technique for different colloidal nanoparticle properties is studied in [57–61].

The main goal of this paper is to explore the possibility of production of colloidal Al-doped (as the promising p-doping candidate) ZnO nanoparticles using LAL technique in water medium. We have particularly focused on the ZnO:Al₂O₃ targets to investigate the possibility of synthesis of Al-doped ZnO nanoparticles which are crucial for optoelectronics applications. In addition, we have varied various experimental conditions in order to optimize the LAL process and the properties of obtained ZnO nanoparticles.

2. Experimental

In this study, we have used a ZnO:Al₂O₃ target (98 wt.% ZnO, 2 wt.% Al₂O₃), for synthesis of colloidal nanoparticles by means of laser ablation in water. The experimental set-up is shown in [62]. The target was immersed in 30 ml beaker containing 28 ml of MilliQ water. The water thickness above the target surface was kept constant at 2 cm during laser ablation in order to keep the laser ablation efficiency constant [63]. Beside MilliQ water that was used as a liquid medium for the most of the syntheses, one experiment was conducted in deionized (DI) water for the comparison. The targets were irradiated by Nd:YAG laser operating at wavelength of $\lambda = 1064$ nm, 5 Hz of repetition rate and pulse durations of 4, 5, 8 and 13 ns for 300, 200, 100 and 50 mJ of output energy, respectively. The energy delivered to the target surface is 40% of output energy. The laser pulse is focused on the target surface immersed in a water using a 10 cm lens. The laser pulse focal plane position is corrected after each 1000 pulses as the index of refraction changes with the time of processing (with number of

Table 1

Laser parameters for 1064 nm of output wavelength and 5 Hz repetition rate.

E_{out} (mJ)	300	200	100	50
E_{target} (mJ)	120	80	40	20
r (μm)	298	297	221	213
Area (10^{-3} cm ²)	2.78	2.77	1.53	1.42
Fluence (J/cm ²)	43	29	26	14
Pulse duration (ns)	4	5	8	13
Power density (GW/cm ²)	10.8	5.7	3.3	1.1

pulses) due to increase of colloidal density. The laser operating parameters for various output energies are summarized in Table 1.

After experiments, the craters created on the targets were studied with an optical microscope (Leitz, Leica Aristomet, reflective illumination mode) in order to determine crater's volume, depth and shape and to assess the nanoparticle synthesis efficiency.

The optical absorbance of laser synthesized colloidal solutions was recorded in the wavelength range from 190 to 800 nm using a UV-Vis spectrophotometer (Lambda 25, Perkin Elmer). The morphology and size-distribution of the obtained nanoparticles was studied by a field emission scanning electron microscope (SEM, Joel 7600F). Specimens for SEM imaging were prepared by depositing one drop of a suspension on a polished Al sample holder. The colloidal solutions were sonicated for 5 min before the deposition. The holder with the specimens was coated with a 3 nm thick carbon layer prior to the SEM imaging. The Al/Zn ratio in ZnO nanoparticles was determined with the FE-SEM equipped with an energy-dispersive X-ray spectrometer (EDXS) elemental analysis system. Specimens for EDXS analysis were prepared by depositing a drop of prepared colloidal suspensions on a carbon tape placed on a carbon sample holder. The holder with the specimens was coated with a thin carbon layer prior to the EDXS analyses. The SEM images were processed by ImageJ software to obtain the size-distributions of Al-doped ZnO nanoparticles.

Films of the colloidal solutions were prepared for XRD (X-ray diffraction) measurements by drop coating of particular solution onto a Si substrate. The dropping was repeated several times until a visible film was formed. Prepared films were structurally examined with GIXRD (grazing incidence X-ray diffraction) technique. The GIXRD measurements were carried out on a diffractometer equipped with a Co X-ray tube and a W/C multilayer for beam shaping and monochromatization. The diffracted spectra were collected with a curved position sensitive detector (RADICON) in the angular range $2\theta = 30\text{--}85^\circ$. In all measurements, a fixed grazing incidence angle of $\alpha_i = 1.5^\circ$ was used.

The X-ray photoelectron spectroscopy (XPS) analyses were carried out on a PHI-TFA XPS spectrometer produced by Physical Electronics Inc. The analyzed area was 0.4 mm in diameter and the analyzed depth was about 3–5 nm. Sample surfaces were excited by X-ray radiation from a monochromatic Al source at photon energy of 1486.6 eV. The high-energy resolution spectra were acquired with an energy analyzer operating at resolution of about 0.6 eV and pass energy of 29 eV. During data processing the spectra from the surface were aligned by setting the C 1s peak at 284.8 eV, characteristic for C–C/H bonds. The accuracy of binding energies was about ± 0.3 eV. Quantification of surface composition was performed from XPS peak intensities taking into account relative sensitivity factors provided by instrument manufacturer [64]. Two different XPS measurements were performed on each sample and average composition was calculated.

Photoluminescence (PL) was measured at room temperature using a continuous wave laser diode at 405 nm. Spectra were collected using a BWTek BCR 112E spectrometer coupled with a Sony ILX511 CCD linear image sensor. Before spectrometer a longpass filter at 450 nm was placed.

3. Results and discussion

In Table 2 beside exact experimental conditions as number of laser pulses and laser energy a band-gap energy Al/Zn ratio, nanoparticles' average diameter and calculated nanoparticle concentration for all samples (marked as sp.1 to sp.8) are given.

3.1. Crater and UV-Vis analyses

During the laser ablation process craters were created in the targets. In order to determine the volume of ablated material (or ablation rate) which is assumed to correspond to the concentration of formed ZnO nanoparticles and to compare it with photoabsorption results the craters have been analyzed and quantified. Additionally, craters were used to get insight into the processes involved in LAL.

In Fig. 1 craters semi-profiles obtained with (a) different number of applied laser pulses with 300 mJ of output energy and (b) obtained with different energies with fixed 10,000 applied laser pulses. It can be seen that craters differ in shape, depth and radius. Such semi-profiles are used for calculation of crater's volumes

(ablated volume) used for calculation of nanoparticle concentrations. The procedure on how the crater volume is determined is described in details in [65]. It can be seen that craters obtained with lower energies (sp.5, sp.6 and sp.7) or with low number of pulses (sp.4) have Gaussian profiles following the laser beam profile. Otherwise, craters profiles obtained with 300 mJ (sp.1, sp.2 and sp.3) deviate from Gaussian profiles possibly due to redeposition of ablated material back onto the crater surface caused by severe ablation. Although the laser ablation in water is known as redeposition-free technique [63,66] while the heat-affected zone is significantly reduced [67] it obviously applies up to some values of laser energies when a water medium cannot carry the ablated material away from the crater efficiently anymore.

UV-Vis absorbance spectra of the Al-doped ZnO colloidal solutions prepared with (a) different number of laser pulses (sp.1, sp.2, sp.3 and sp.4) and (b) different laser output energies (sp.2, sp.5, sp.6 and sp.7) is shown in Fig. 2. In Fig. 2(a) a UV-Vis spectrum of pure ZnO colloidal solution is shown for comparison (red dotted line) obtained with 300 mJ and 10,000 laser pulses (like sp.2 sample). It can be seen that absorbance maximum at 330 nm is 30% lower than that of sp.2 sample indicating that nanoparticle

Table 2

Sample labels, experimental conditions (pulse number and laser output energy) and properties of the studied samples (Al/Zn ratio and band gap values).

Sample notation	Number of pulses	Laser energy (mJ)	Band-gap (eV)	Average diameter (nm)	Al/Zn ratio**	Concentration*** (10^9 ml^{-1})
sp.1	15,000	300	3.31	509	0.12 ± 0.02	1.9 ± 0.2
sp.2	10,000	300	3.29	502	0.15 ± 0.03	1.4 ± 0.1
sp.3	5000	300	3.27	481	0.15 ± 0.02	1.0 ± 0.1
sp.4	2500	300	3.17	453	0.17 ± 0.03	0.6 ± 0.1
sp.5	10,000	200	3.31	496	0.13 ± 0.01	1.5 ± 0.2
sp.6	10,000	100	3.26	499	0.16 ± 0.02	0.9 ± 0.1
sp.7	10,000	50	3.15	495	0.33 ± 0.07	0.38 ± 0.05
sp.8*	10,000	300	3.09	234	0.14 ± 0.02	-

* Sample sp.8 was prepared in deionised water while all the others in MilliQ water.

** Al/Zn ratio was calculated from the data obtained from EDXS.

*** Concentration was calculated from the crater volumes and average sizes of nanoparticles.

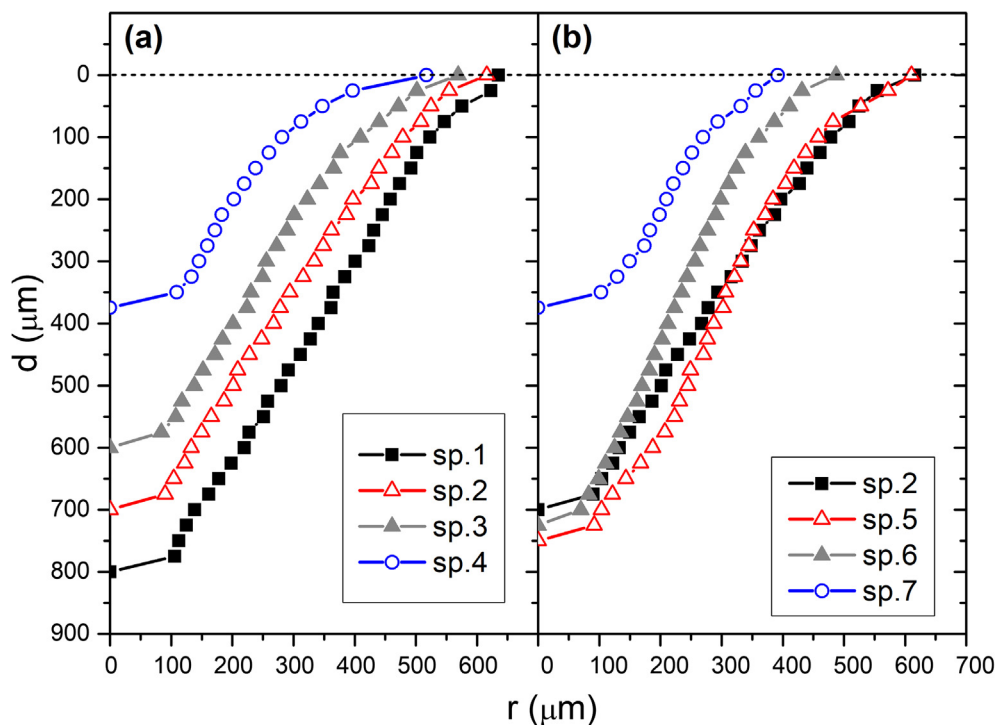


Fig. 1. Craters semi-profiles obtained with different (a) number of laser pulses and (b) different laser energies.

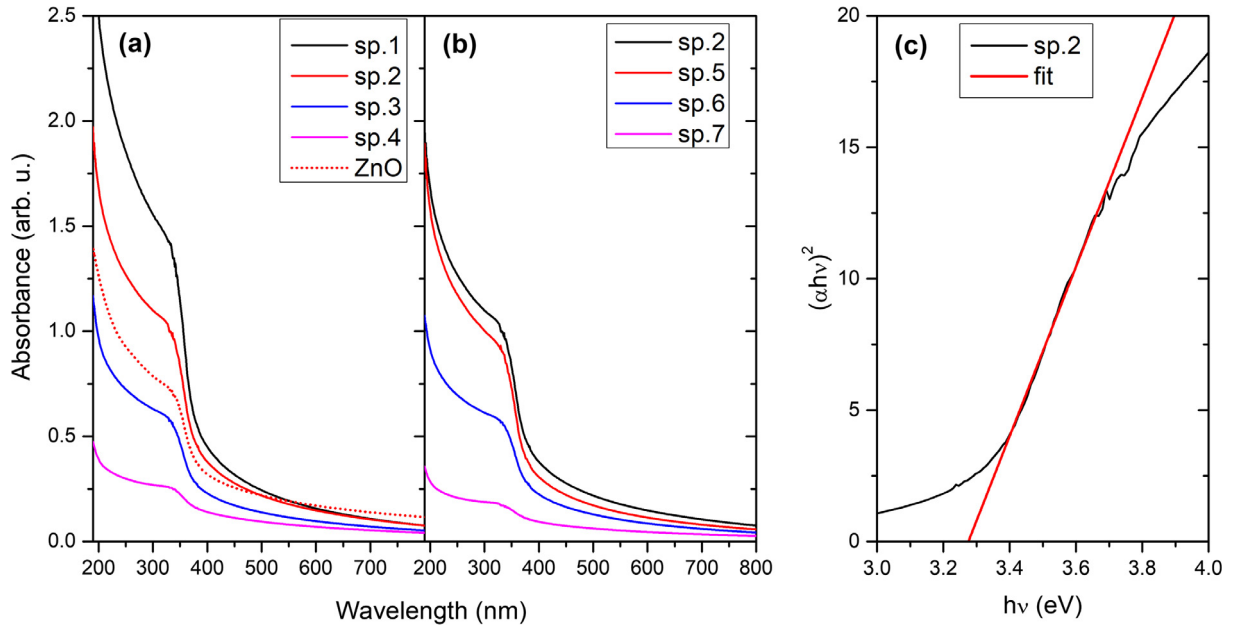


Fig. 2. UV-vis spectra of colloidal solutions as a function of (a) number of pulses and (b) laser output energy. In (a) is shown photoabsorption for colloidal solution of pure ZnO nanoparticles for comparison (red dotted line). In (c) $(\alpha h\nu)^2$ versus photon energy for sample sp.2 is shown (black line) with a linear fit (red line) to obtain the band-gap energy. (For interpretation of the references to colour in this figure legend, the reader is referred to the web version of this article.)

production rate is higher for Al-doped ZnO samples. All spectra in Fig. 2(a) and (b) show a characteristic sharp curve (within 330 and 400 nm) including distinct maximum at 330 nm typical for ZnO nanoparticles [68] positioned between low absorption in visible part of the spectrum and high absorption in UV part. The higher the number of applied laser pulses the sharper the absorption curve. This also applies for all output energies except that for 300 mJ which is similar to 200 mJ case. From photoabsorption spectra shown in Fig. 2(a) and (b) a ZnO band-gap can be determined. Details on band-gap calculation can be found in [62]. As an example, the calculated band-gap is shown in Fig. 2(c) for the sp.2 case and its value is 3.29 eV.

In Fig. 3 a comparison of calculated crater volume (left y-axis) and absorbance at 330 nm of ZnO:Al₂O₃ (right y-axis) as a function of (a) laser pulses and (b) output energy is shown. Craters were obtained from crater semi-profiles shown in Fig. 1 while absorbances were extracted from UV-Vis spectra shown in Fig. 2. It can be seen in Fig. 3(a) that both volumes and absorbances increase linearly with the number of applied laser pulses. It implies that volumes and absorbance are interrelated as most of ablated material appeared in a form of absorbing (absorption and scattering) nanoparticles. Otherwise, if that is not the case, the ablated material would have significant amount of debris and other, wavelength independent scatterers so the absorption curve would have different, rather complicated shape than that presented in Fig. 2. Moreover, its relative intensity at 330 nm vs. number of pulses will not follow the same trend as shown in Fig. 3(a). Again, both volumes and absorbances have the same dependence on energy as is shown in Fig. 2(b) confirming close relation between the volume of ablated material and absorbance. That leads us to an assumption that ablated volume in most of its part is transferred into nanoparticles upon LAL within used parameter space.

Band-gap energies for Al-doped ZnO nanoparticles as a function of number of applied laser pulses, laser pulse energy and type of water are shown in Table 2. The band-gaps are of lower values (red-shifted) in comparison to the reported values [69–71] but they exhibit slight increase with both number of applied laser pulses and laser output energy. The reported values of bulk

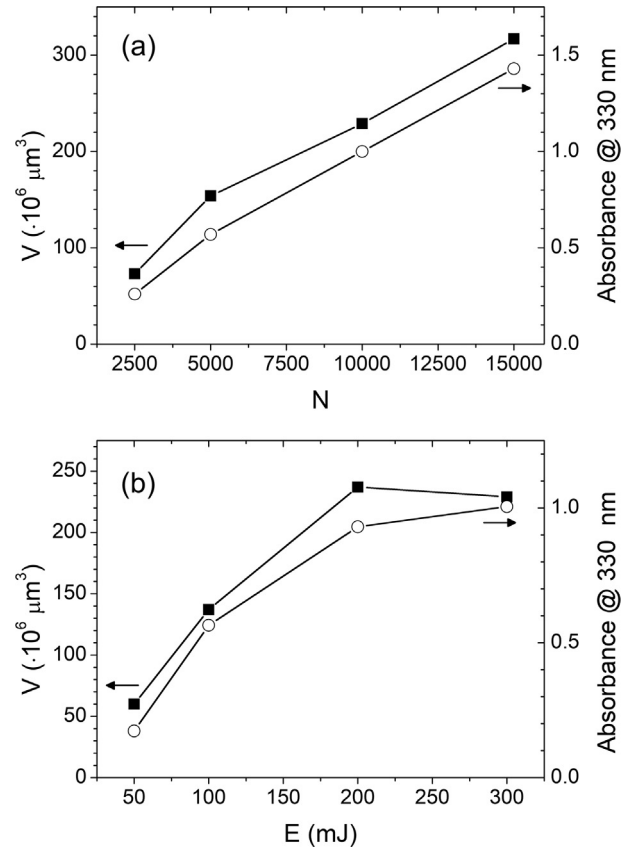


Fig. 3. Crater volumes (left, black squares) and maximum absorbance (right, empty circles) as a function of (a) number of pulses and (b) laser output energies.

ZnO are in the range from $E_g = 3.3$ to 3.82 eV, depending on the crystal properties, synthesis routes and measurement techniques. The band-gap closest to the reported values is observed for the nanoparticles synthesized with larger number of pulses or high

laser energy output; samples sp.1, sp.2 and sp.5. The lowest band-gap of 3.09 eV was measured for the nanoparticles that were synthesized in DI water (sp.8). So the high laser output energies and number of applied laser pulses favour synthesis of Al-doped ZnO nanoparticles with band-gap closest to the bulk value. The red-shift of the obtained band-gaps is likely ascribed to the size and shape of nanoparticles, defects in energy levels, impurities and structural defects [72]. Moreover, UV-Vis spectroscopy showed that doped ZnO material exhibit band gap narrowing both in the nano and micro states with respect to the pure ZnO material [73].

3.2. GIXRD analysis

The crystallinity of the Al-doped ZnO nanoparticles was examined by GIXRD measurements. The selected GIXRD spectra for the samples sp.2, sp.7 and sp.8, together with the reference patterns for the ZnO and Al₂O₃ phases, are shown in Fig. 4. As can be seen, the experimental GIXRD spectra of all samples show only the peaks characteristic for the hexagonal wurtzite phase of ZnO. In addition, the presence of all main ZnO diffraction peaks in the experimental curves indicate randomly oriented crystallites within the film (no preferential orientation). The main difference among spectra shown in Fig. 4 is noticeable less intense diffraction peaks for the sp.8 sample, indicating lower number of crystallites present within this sample.

Furthermore, a lack of Al₂O₃ diffraction peaks in the GIXRD spectra, at least the most intense ones, discards the laser-prepared colloidal solutions as a heterogeneous mixture of ZnO and Al₂O₃ phases. This indicates that the Al₂O₃ phase is dissolved within the ZnO crystallites. The intensity of Al₂O₃ peaks may be below the sensitivity of GIXRD method. However, GIXRD spectra cannot be used to identify whether the Al₂O₃ is doped in ZnO nanoparticles or not so further measurements were carried out (XPS and EDSX) to identify that issue.

3.3. SEM analysis

A SEM imaging was used to determine the impact of the synthesis parameters such as number of laser pulses, laser output energy and type of water on the morphology of nanoparticles and to determine its size-distribution. In Fig. 5 a characteristic SEM images of (a) sp.2, (b) sp.5, (c) sp.3 and (d) sp.8 are shown. It can be seen that at all synthesis conditions, except for the DI water, the formed nanoparticles are in the shape of 2D discs with the diameters

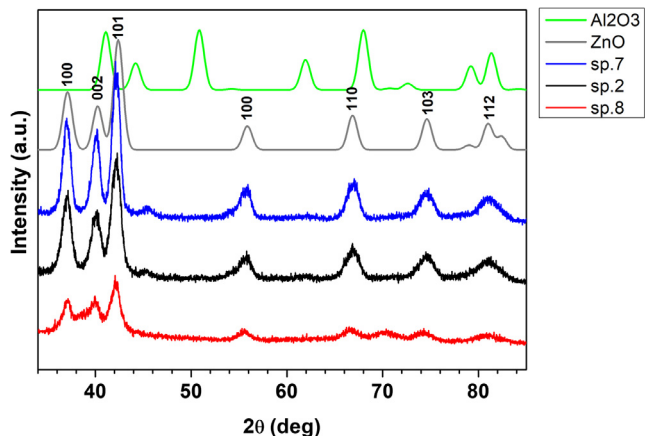


Fig. 4. XRD patterns of Al-doped ZnO nanoparticles for sp.7, sp.2 and sp.8 samples. The top most spectra are a reference XRD spectra of ZnO and Al₂O₃. Spectra were equidistantly separated for better visibility.

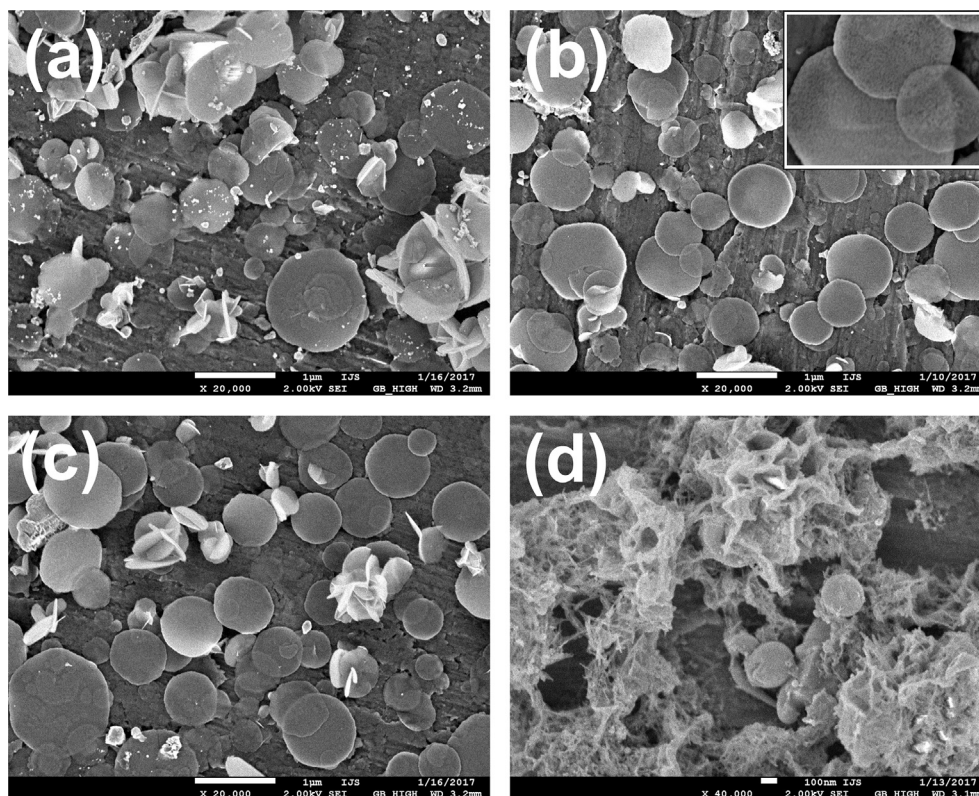


Fig. 5. SEM images of Al-doped ZnO nanoparticles for samples (a) sp.2, (b) sp.5, (c) sp.3 and (d) sp.8. (a)–(c) images were taken at the same magnification of 20,000× (scale bar is 1 μm) while (d) was taken with 40,000× (Scale bar is 100 nm).

ranging from 100 nm to 1.4 μm . The average thickness of disc-like nanoparticles is (29 ± 3) nm. Inset in Fig. 5(b) is showing a characteristic thin disc-like structure. The obtained Al-doped ZnO nanoparticles are of core/shell structure with crystalline core and amorphous 5 nm thick shell as was found with TEM imaging [62]. Morphology of the sample synthesized in DI water is rather different in comparison to all other samples as shown in Fig. 5 (d). It appears that 3D mesh-like structures with sparse concentration of colloidal nanoparticles were obtained. Thus, from the point of production rate of colloidal nanoparticles by LAL and purity of the colloidal samples, a MilliQ is more favourable than DI water. Average diameter of all nanoparticles is shown in Table 2 and its value is ranging from 450 to 550 nm in synthesis in MilliQ water, while that for DI water is 234 nm. It is worthwhile to note that nanoparticles diameter does not depend on applied laser pulse energy but only on number of laser pulses.

ZnO nanoparticle formation processes in LAL are described with dynamical formation mechanisms including diffusion growth process or diffusion coalescence process [74–76]. The formation of disc-like Al-doped ZnO nanoparticles may be ascribed to two processes defining the growth of such nanoparticles [77]. The first is that it was found that ions from the laser ablated plasma plume may dominate the growth of nanoparticles as dopant particles (in our case that would be Al) [78]. The second is that the nanoparticle growth upon LAL is defined by the surface energy of the formed crystals with different orientation which may result in preferential formation of nanodiscs (we revealed by XPS that formed nanodiscs are comprised of randomly oriented crystallites). Moreover, pressure and temperature gradients may also induce 2D anisotropic directional growth [79] as well as the high-temperature nucleation [80]. There is still no verification for final mechanism of disc-like Al-doped ZnO growth.

The elemental composition of the nanoparticles was carried out by energy dispersive X-ray spectroscopy (EDXS). The results of the Al/Zn ratio in dependence of energy and number of pulses are shown in Table 2. In general, the Al/Zn ratio shows very weak dependence on number of laser pulses or on laser output energy except for the lowest energy of 50 mJ (sp.7). In this case the value is very similar to the Al/Zn value of the target. Note that when doping is increasing the band-gap is decreasing. The same behaviour is found in [81] and it is related to crystal size increase and lattice strain decrease. Interestingly, the Al/Zn values for all the samples are lower than that of the Al/Zn ratio in the target, except that for sp.7. This might be explained by leaching of aluminium from the nanoparticles to the liquid phase during and after the synthesis (the samples for EDXS analysis were prepared a week after the synthesis) [82]. It is well known that laser ablation within such high pulse energy range allows for stoichiometric ablation, i.e. the stoichiometry of bulk is reflected into stoichiometry of ablated plasma plume [83] (from which further nanoparticle growth takes place). So, if stoichiometry from target to the ZnO nanoparticles synthesized by LAL of ZnO:Al₂O₃ in MilliQ water needs to be preserved it is obvious that lower laser output energies should be used. From these results we can conclude that by regulation of laser ablation parameters, especially the laser output energy, we can tailor the aluminium content in the ZnO nanoparticles to some extent.

3.4. XPS and photoluminescence analysis

Elemental composition of synthesized nanoparticles is determined with XPS and shown in Table 3 for selected characteristic samples (sp.2, sp.4 and sp.7). It is shown that small amount of Al presented in nanoparticles is detected with XPS while Al/Zn ratio shows the same relative trend as that obtained with EDXS but with smaller values (in both cases Al/Zn ratio increases either decreasing the number of laser pulses or decreasing the laser output

Table 3

XPS elemental compositions and Al/Zn and O/Zn ratios of samples sp.2, sp.4 and sp.7.

Sample \ element	O 1s (at.%)	Al 2p (at.%)	Zn 2p (at.%)	Al/Zn	O/Zn
sp.2	58.9	2.5	38.6	0.07	1.53
sp.4	63.2	4.2	32.6	0.13	1.93
sp.7	68	5.9	26.1	0.23	2.6

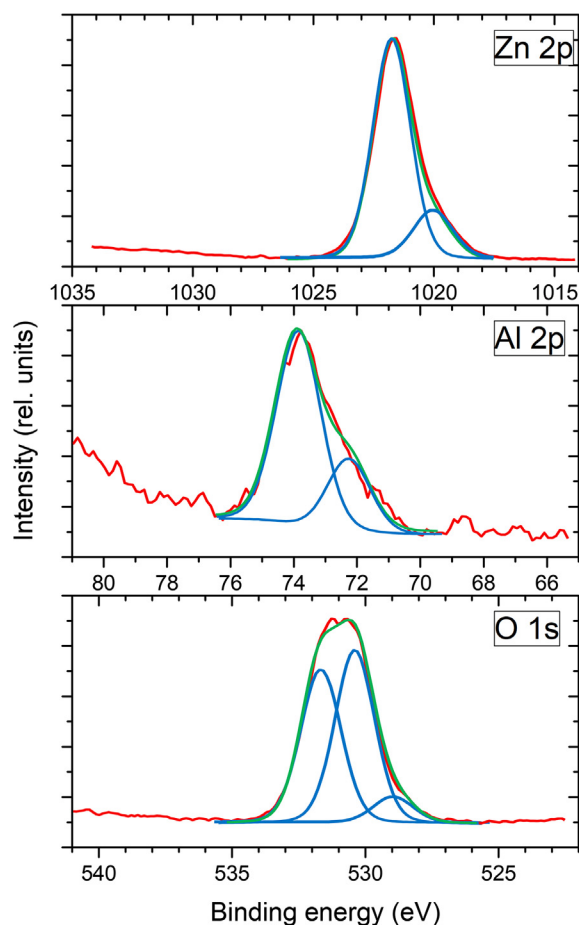


Fig. 6. High resolution XPS spectra of Zn 2p, Al 2p and O 1s (red line) with fit spectra (blue and green) of sample sp.4. (For interpretation of the references to colour in this figure legend, the reader is referred to the web version of this article.)

energy). The higher Al/Zn ratio is obtained with lowest laser output energy (sp.7) like it was found with EDXS. The increase in Al atomic concentration and O/Zn ratio is also observed (smallest for sp.2, highest for sp.7). In Fig. 6 high resolution XPS spectra from sample sp.4 for Zn 2p fitted with two components at 1019.9 eV (15%) and 1021.7 eV (85%), Al 2p fitted with two components at 72.3 eV (27%) and 73.9 eV (73%) and O 1s fitted with three components at 528.9 eV (6%), 530.3 eV (50%) and 531.7 eV (43%). XPS spectra are qualitatively similar for all measured samples (sp.2, sp.4 and sp.7). The Zn 2p component at 1021.7 eV corresponds to Zn²⁺ states in ZnO while that at 1019.9 eV may correspond to maybe Zn–Al bonding. The Al 2p component at 72.3 eV corresponds to Al(0) states. This component is probably related with doped Al-atoms in ZnO phase. The Al 2p component at 73.9 eV corresponds to Al³⁺ states like in Al₂O₃ compound. It is probably related with the oxidized surface. The O 1s components at 528.9 eV and 530.3 eV correspond to O²⁻ states. These components are probably related with oxide lattice in ZnO phase. The O 1s component at 531.7 eV may be associated with O²⁻ ions in the oxygen deficient regions within the

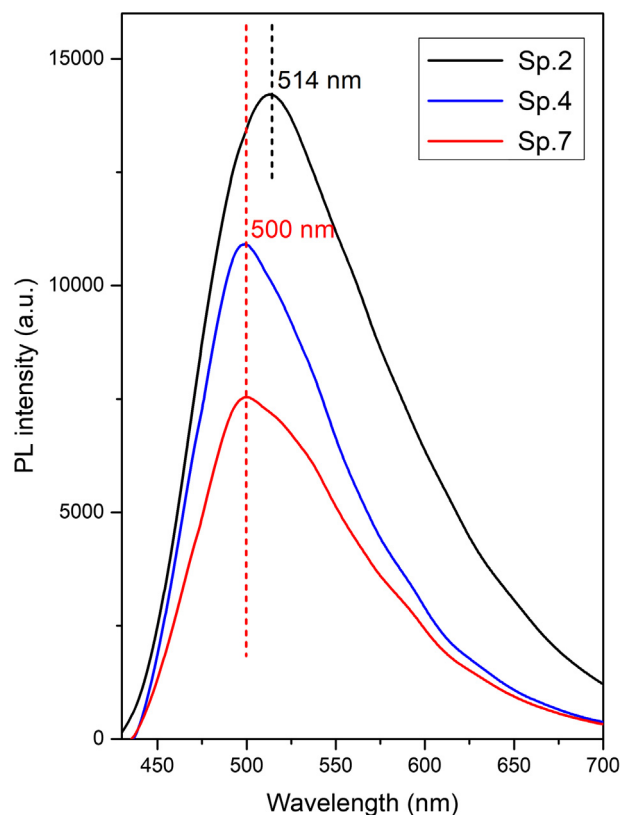


Fig. 7. Photoluminescence of sp.2, sp.4 and sp.7.

matrix of ZnO and therefore with concentration of oxygen vacancies [84]. Another possible assignment of this component might be assigned to chemisorbed oxygen ions.

Fig. 7 presents the photoluminescence spectra of samples sp.2, sp.4 and sp.7, showing broad luminescence band peaking at 514 nm for sp.2 and 500 nm for sp.4 and sp.7. The green PL is due to transitions between conduction band and deep level defects [85] ascribed to a presence of oxygen vacancies [86]. The highest PL intensity shows sp.2 sample with red-shifted maximum with respect to two other samples while PL intensity of sp.7 sample is the lowest, twice lower than sp.2. It was found with XPS that the surface concentration of oxygen is lowest for sp.2 case and highest for sp.7 case (Table 3) which confirm the PL spectra. The lowest concentration of oxygen implies consequently that the concentrations of oxygen vacancies in the lattice is highest which, upon recombination with electrons, emit green PL [87].

3.5. Size-distribution of ZnO colloidal nanoparticles

Size-distribution of nanoparticles is determined using SEM images. In Fig. 8 size-distributions of nanoparticles synthesized for samples sp.1, sp.4 and sp.8 are shown. Size distributions are obtained by analysing 583 and 157 and 75 particles, respectively. The size-distributions were fitted with Log Normal (LogN) curve (black line) in order to obtain the peak maximum of the distribution. The maximum of the LogN distribution (average diameter) are shown in Table 2 for all samples. The LogN fit is often used to describe the size-distribution of the nanoparticles synthesized from gaseous phase what is the case in nanoparticles syntheses processes by LAL. It applies whenever particle growth depends on diffusion and drift of atoms to a growth zone of nanoparticles [88]. The final distribution is determined with the available growth time of the nanoparticles [89]. It can be seen from Fig. 8 that size of

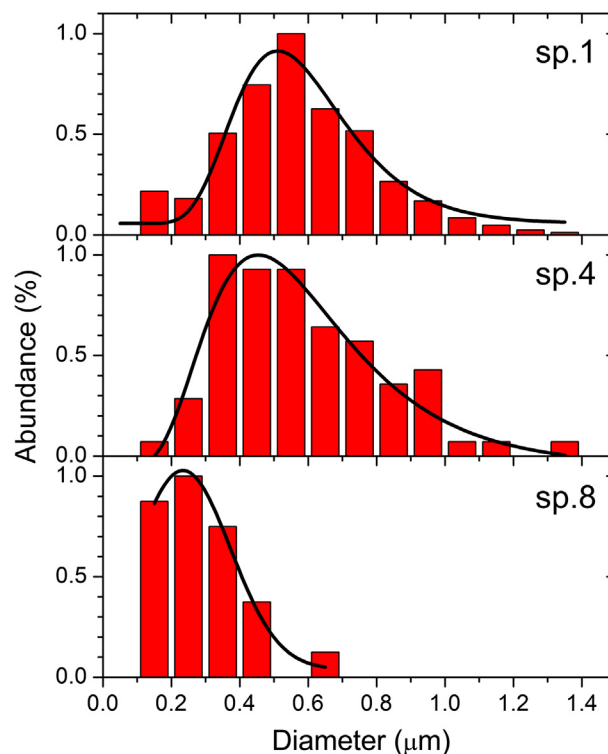


Fig. 8. The nanoparticles size-distributions of sp.1, sp.4 and sp.8 samples (column bars) with corresponding LogNormal fit (solid line).

nanoparticles depends on number of applied pulses ranging from 453 nm to 509 nm for 2500 (sp.4) and 15,000 (sp.1) pulses, respectively. On the other side, size-distribution does not depend on laser pulse energy although the crater volume and absorbance depend on it as is shown in Figs. 2 and 3. The average diameter of nanoparticles synthesized in DI water is 234 nm.

The size of particles is independent on laser output energy although the crater volume and absorbance depend on it as shown in Figs. 4(b) and 6(b), respectively. In [88] it was found that ZnO nanoparticle size is not influenced by the laser fluence (corresponding to the laser pulse energy) nor by ablation time (corresponding to the number of laser pulses) upon synthesis of ZnO nanoparticles by laser ablation in DI water under similar experimental conditions. The only difference from our case was that during LAL the target was moving in order to avoid drilling and possible heating effects. It leads to the conclusion that in our case the crater influences the particle size (which volume corresponds to the number of applied laser pulses). The dependence of particle size on number of applied laser pulses may be ascribed to the continuous heating of the target upon prolonged laser ablation as the laser pulse was impinging the same spot during LAL so the energy threshold for the ablation decreases promoting the ablation rate and thus density of ablated species in gaseous phase. But that is less-likely scenario as there is no evidence to support it. From the dependence of volumes of craters and photoabsorption intensity on number of applied laser pulses such conclusion could not be made because volumes and photoabsorption will increase with the number of pulses rather exponentially than linearly as was found here. The more-likely scenario is that upon laser ablation the craters becoming larger and deeper so the ablated material is bounded by its walls and it does not have much space to spread around. When laser pulse impinges onto the target a dynamic plasma plume consisting of the ions, atoms and molecules is formed and it expands. The formation of ZnO particles can be described with dynamic formation mechanism [74], as was

discussed earlier, from the plasma plume which includes rapid growth (initial stage of formation, ps-ns range) of ZnO clusters in the laser plasma plume which are nuclei for further slow growth (intermediate stage of formation, ns range) due to diffusion of particles in the vicinity of the clusters. Further coagulation and coalescence, if growth is not affected by surfactants [75,90], takes place (late stage of formation, ns-ms range) leading to the possible agglomerations and precipitations. If the growth of particles from gaseous phase is spatially restricted, this increases the probability for the diffusion of surrounding particles to the vicinity of embryonic particles, which results in a formation of larger nanoparticles at a final stage of its growth. In other words, the diffusion length of the gaseous particles (Zn, O and Al atoms and ions) to the embryonic particle is smaller. It is assumed that larger nanoparticles are formed in deeper craters due to higher density of ablated gaseous material in spatially restricted volume involved in nanoparticles growth (higher probability of growth of larger nanoparticles).

3.6. Concentration of nanoparticles

Concentration of nanoparticles is calculated from known volumes of ablated material (volume of a crater) and average volume of single nanoparticle. The calculation is made under the assumption that whole crater volume is transferred into nanoparticles neglecting the possibility that part of ablated material appeared as debris. The nanoparticles were assumed as discs of average diameters given by the size-distribution and thicknesses obtained from SEM images. There was no distinction in thicknesses among nanoparticles obtained with different synthesis parameters. The average nanoparticles thickness is 29 ± 3 nm. The concentration of nanoparticles is calculated as ratio of crater volume (given in Fig. 3) and average nanoparticle volume divided by 28 ml of water used for the synthesis.

For example, sample sp.1 has average nanoparticle diameter of 509 nm giving the average volume of disc-like single nanoparticle of $V_{sp1} = 5.9 \cdot 10^{-3} \mu\text{m}^3$. Corresponding crater volume is $V_{c,sp1} = 317 \cdot 10^6 \mu\text{m}^3$. The ratio $N = V_{c,sp1}/V_{sp1}$ gives a total number of nanoparticles created from crater volume to be $5.37 \cdot 10^{10}$. The synthesis was performed in 28 ml of MilliQ water so the concentration is $n = N/28 \text{ ml} = 1.9 \cdot 10^9 \text{ ml}^{-1}$. The nanoparticles concentrations for all samples are listed in Table 2. Exception is sp.8 where assumption that most of ablated material is transferred into nanoparticles is not valid due to a presence of dominating mesh-like structures.

4. Conclusion

In summary, we have successfully synthesized colloidal solutions of Al-doped ZnO nanoparticles by LAL technique performed in MilliQ water. The formed disc-like nanoparticles have thickness of 29 nm and diameter ranging from 450 to 510 nm. It was found that the size of colloidal particles depends on the number of applied laser pulses but not on the laser pulse energy. It is explained by the fact that growth takes place in spatially restricted volume of the target crater. The boundary of the crater supports the diffusion-growth of particles as the density of Zn and O atoms is high thus statistically increasing the possibility of adsorption on the embryonic (nucleus) particle. The XRD analysis revealed that all synthesized ZnO particles are crystalline. The XPS analyses recognized different chemical states of Zn, Al and O atoms in synthesized nanoparticles. Zn atoms are mainly present as Zn^{2+} in ZnO phase while speculating a small presence of Zn-Al bonded atoms was revealed. Al atoms are present partially in metallic state what is probably related with the doped Al atoms in ZnO phase. In addition, Al atoms in (3+) oxidation state were detected originating from oxidized sample surface.

The synthesis in DI water reveal sparse density of nanoparticles with dominating mesh-like structures.

When energy and number of laser pulses are high enough the synthesized nanoparticles are of high concentration, band-gap is close to the pure ZnO, there is no significant doping level and PL spectra show intense green PL. When the number of laser pulses is small both the band-gap and the Al/Zn ratio are relatively small. Finally, when the energy of laser pulses is small the band-gap and concentration are small but Al/Zn ratio is reaching a bulk value. To tune the properties of synthesized ZnO nanoparticles with LAL there is an interplay between low laser energy and low number of applied laser pulses.

We demonstrated how to obtain the concentration of colloidal nanoparticles from known size-distribution and a crater volume.

In this work we showed how the properties of Al-doped ZnO nanoparticles synthesized by LAL can be adjusted within a parameter space used. We also promoted LAL as efficient Al-doped ZnO nanoparticle colloidal synthesis technique for various applications.

Acknowledgements

This work has been supported in part by the Croatian Science Foundation under the Project IP-11-2013-2753 and in part by the Slovenian Research Agency research programs P1-0125 and P2-0082. NK acknowledge the COST Action TD 1208 for fruitful discussions. Authors would like to thank Tatjana Filipič performing XPS analyses.

References

- [1] N.V. Tarasenko, A.V. Butsen, Laser synthesis and modification of composite nanoparticles in liquids, *Quantum Electron.* 40 (2010) 986–1003.
- [2] S. Barcikowski, F. Mafuné, Trends and current topics in the field of laser ablation and nanoparticle generation in liquids 4985 *J. Phys. Chem. C* 115 (2011).
- [3] G. Yan, *Laser Ablation in Liquids: Principles and Applications in the Preparation of Nanomaterials*, Pan Stanford Publishing, Singapore, 2012.
- [4] H. Zeng, X.-W. Du, S.C. Singh, S.A. Kulnich, S. Yang, J. He, W. Cai, *Nanomaterials via laser ablation/irradiation in liquid: A review*, *Adv. Funct. Mater.* 22 (2012) 1333–1353.
- [5] D. Zhang, B. Gökce, Stephan Barcikowski, *Laser synthesis and processing of colloids: fundamentals and applications*, *Chem. Rev.* 117 (117) (2017) 3990–4103.
- [6] S. Besner, A.V. Kabashin, F.M. Winnik, M. Meunier, Ultrafast laser based "green" synthesis of non-toxic nanoparticles in aqueous solutions, *Appl. Phys. A* (2008) 955–959.
- [7] N. Bärsch, J. Jakobi, S. Weiler, S. Barcikowski, Pure colloidal metal and ceramic nanoparticles from high-power picosecond laser ablation in water and acetone, *Nanotechnology* 20 (445603) (2009) 1–9.
- [8] J. Zhang, M. Post, T. Veres, Z.J. Jakubek, J. Guan, D. Wang, F. Normandin, Y. Deslandes, B. Simard, Laser-assisted synthesis of superparamagnetic Fe@Au core-shell nanoparticles, *J. Phys. Chem. B* 110 (2006) 7122–7128.
- [9] A. De Bonis, A. Galasso, A. Santagata, R. Teghil, Laser ablation of GaAs in liquid: the role of laser pulse duration, *J. Phys. D: Appl. Phys.* 49 (2016) 035301–35307.
- [10] K.V. Anikin, N.N. Melnik, A.V. Simakin, G.A. Shafeev, V.V. Voronov, A.G. Vitukhnovsky, Formation of ZnSe and CdS quantum dots via laser ablation in liquids, *Chem. Phys. Lett.* 366 (2002) 357–360.
- [11] N.G. Semaltianos, S. Logothetidis, W. Perrie, S. Romani, R.J. Potter, M. Sharp, G. Dearden, K.G. Watkins, CdTe nanoparticles synthesized by laser ablation, *Appl. Phys. Lett.* 95 (2009) 033302.
- [12] M. Tsuji, S. Kuboyama, T. Matsuzaki, T. Tsuji, Formation of hydrogen-capped polyynes by laser ablation of C_{60} particles suspended in solution, *Carbon* 41 (2003) 2141–2148.
- [13] G. Compagnini, V. Mita, L. D'Urso, R.S. Cataliotti, O. Puglisi, Spectroscopic study of polyynes obtained by laser ablation in liquids, *J. Raman. Spectrosc.* 39 (2008) 177–181.
- [14] V. Amendola, P. Riello, M. Meneghetti, Magnetic nanoparticles of iron carbide, iron oxide, iron@iron oxide, and metal iron synthesized by laser ablation in organic solvents, *J. Phys. Chem. C* 115 (2011) 5140–5146.
- [15] N.V. Tarasenko, A.V. Butsen, M.I. Nedelko, N.N. Tarasenko, Laser-aided preparation and modification of gadolinium silicide nanoparticles in liquid, *J. Phys. Chem. C* 116 (2012) 3897–3902.
- [16] D. Zhang, B. Gökce, Perspective of laser-prototyping nanoparticle-polymer composites, *Appl. Surf. Sci.* 392 (2017) 991–1003.

- [17] D. Zhang, J. Liu, P. Li, Z. Tian, C. Liang, Recent advances in surfactant-free, surface charged and defect-rich catalysts developed by laser ablation and processing in liquids, *ChemNanoMat*. 10.1002/cnma.201700079.
- [18] D. Zhang, B. Gökce, C. Notthoff, S. Barcikowski, Layered seed-growth of AgGe football-like microspheres via precursor-free picosecond laser synthesis in water, *Sci. Rep.* 5 (2015) 13661.
- [19] S.I. Dolgaev, A.V. Simakin, V.V. Voronov, G.A. Shafeev, F. Bozon-Verduraz, nanoparticles produced by laser ablation of solids in liquid environment, *Appl. Surf. Sci.* 186 (2002) 546–551.
- [20] T. Tsuji, N. Watanabe, M. Tsuji, Laser induced morphology change of silver colloids: formation of nano-size wires, *Appl. Surf. Sci.* 211 (2003) 189–193.
- [21] T. Tsuji, Y. Okazaki, T. Higuchi, M. Tsuji, Laser-induced morphology changes of silver colloids prepared by laser ablation in water enhancement of anisotropic shape conversions by chloride ions, *J. Photochem. Photobiol. A* 183 (2006) 297–303.
- [22] H. Zeng, S. Yang, W. Cai, Reshaping formation and luminescence evolution of ZnO quantum dots by laser-induced fragmentation in liquid, *J. Phys. Chem. C* 115 (2011) 5038–5043.
- [23] E. Giorgetti, F. Giammanco, P. Marsili, A. Giusti, Effect of picosecond postirradiation on colloidal suspensions of differently capped AuNPs, *J. Phys. Chem. C* 115 (2011) 5011–5020.
- [24] V.S. Burakov, N.V. Tarasenko, A.V. Butsen, V.A. Rozantsev, M.I. Nedel'ko, Formation of nanoparticles during double-pulse laser ablation of metals in liquids, *Eur. Phys. J. Appl. Phys.* 30 (2005) 107–112.
- [25] A. DeGiacomo, A. DeBonis, M. Dell'Aglio, O. De Pascale, R. Gaudiuso, S. Orlando, A. Santagata, G.S. Senesi, F. Taccogna, R. Teghil, Laser ablation of graphite in water in a range of pressure from 1 to 146 atm using single and double pulse techniques for the production of carbon nanostructures, *J. Phys. Chem. C* 115 (2011) 5123–5130.
- [26] M. Dell'Aglio, R. Gaudiuso, R. El Rashedy, O. De Pascale, G. Palazzo, A. De Giacomo, Collinear double pulse laser ablation in water for the production of silver nanoparticles, *Phys. Chem. Chem. Phys.* 15 (2013) 20868–20875.
- [27] D. Werner, S. Hashimoto, Improved working model for interpreting the excitation wavelength- and fluence-dependent response in pulsed laser-induced size reduction of aqueous gold nanoparticles, *J. Phys. Chem. C* 115 (2011) 5063–5072.
- [28] Z. Zang, X. Zeng, J. Du, M. Wang, X. Tang, Femtosecond laser direct writing of microholes on roughened ZnO for output power enhancement of InGaN light-emitting diodes, *Opt. Lett.* 41 (2016) 3463–3466.
- [29] C. Li, C. Han, Y. Zhang, Z. Zang, M. Wang, X. Tang, J. Du, Enhanced photoresponse of self-powered perovskite photodetector based on ZnO nanoparticles decorated CsPbBr₃ films, *Sol. Energy Mater. Sol. Cells* 172 (2017) 341–346.
- [30] R. Kumar, O. Al-Dossary, G. Kumar, A. Umar, *Nano-Micro Lett.* 7 (2015) 97.
- [31] S.Y. Li, C.Y. Lee, T.Y. Tseng, Copper-catalyzed ZnO nanowires on silicon (1 0 0) grown by vapor-liquid-solid process, *J. Cryst. Growth* 247 (2003) 357–362.
- [32] V.M. Markushev, M.V. Ryzkov, C.M. Briskina, *Appl. Phys. A* 84 (2006) 333.
- [33] C. Li, Z. Zang, C. Han, Z. Hu, X. Tang, J. Du, Y. Leng, K. Sun, Enhanced random lasing emission from highly compact CsPbBr₃ perovskite thin films decorated by ZnO nanoparticles, *Nano Energy* 10.1016/j.nanoen.2017.08.013.
- [34] A. Moezzu, A.M. McDonagh, M.B. Cortie, Zinc oxide particles: Synthesis, properties and applications, *Chem. Eng. J.* 1 (2012) 185–186.
- [35] M.S. Ghamsari, S. Alamdari, W. Hana, H.-H. Park, Impact of nanostructured thin ZnO film in ultraviolet protection, *Int. J. Nanomed.* 12 (2017) 207–216.
- [36] M. Gorjanc, K. Jazbec, M. Šala, R. Zaplotnik, A. Vesel, M. Mozetič, Creating cellulose fibres with excellent UV protective properties using moist CF4 plasma and ZnO nanoparticles, *Cellulose* 21 (2014) 3007–3021.
- [37] U. Ozgur, Ya.I. Alivov, C. Liu, A. Teke, M.A. Reshchikov, S. Dogan, V. Avrutin, S.J. Cho, H. Morkoc, A comprehensive review of ZnO materials and devices, *J. Appl. Phys.* 98 (2005) 041301–42100.
- [38] H. Kim, A. Cepler, C. Cetina, D. Knies, M.S. Osofsky, R.C.Y. Auyeung, A. Pique, Pulsed laser deposition of Zr–N codoped p-type ZnO thin films, *Appl. Phys. A* 93 (2008) 593–598.
- [39] X. Wang, Y.M. Lu, D.Z. Shen, Z.Z. Zhang, B.H. Li, B. Yao, J.Y. Zhang, D.X. Zhao, X. W. Fan, Growth and photoluminescence for undoped and N-doped ZnO grown on 6H-SiC substrate, *J. Lumin.* 122–123 (2007) 165–167.
- [40] E.-C. Lee, Y.-S. Kim, Y.-G. Jin, K.J. Chang, Compensation mechanism for N acceptors in ZnO, *Phys. Rev. B* 64 (2001), 085120-1-5.
- [41] A.F. Kohan, G. Ceder, D. Morgan, C.G. Van de Walle, First-principles study of native point defects in ZnO, *Phys. Rev. B* 61 (2000) 15019–15027.
- [42] P.M. Aneesh, M.R. Shijeesh, Arun Aravind, M.K. Jayaraj, Highly luminescent undoped and Mn-doped ZnS nanoparticles by liquid phase pulsed laser ablation, *Appl. Phys. A* 116 (2014) 1085–1089.
- [43] D. Katsuki, T. Sato, R. Suzuki, Y. Nanai, S. Kimura, T. Okuno, Red luminescence of Eu³⁺ doped ZnO nanoparticles fabricated by laser ablation in aqueous solution, *Appl. Phys. A* 108 (2012) 321–327.
- [44] Y.-S. Cho, Y.-D. Huh, C.R. Park, Y.R. Do, Preparation with laser ablation and photoluminescence of Y₃Al₅O₁₂: Ce nanophosphors, *Electron. Mater.* 10 (2014) 461–465.
- [45] F. Yoshimura, K. Nakamura, F. Wakai, M. Hara, M. Yoshimoto, O. Odawara, H. Wada, Preparation of long-afterglow colloidal solution of Sr₂MgSi₂O₇: Eu²⁺, Dy³⁺ by laser ablation in liquid, *Appl. Surf. Sci.* 257 (2011) 2170–2175.
- [46] B. Zhou, B. Shi, D. Jin, X. Liu, Controlling upconversion nanocrystals for emerging applications, *Nat. Nanotechnol.* 10 (2015) 924–936.
- [47] T. Nunokawa, Y. Onodera, M. Hara, Y. Kitamoto, O. Odawara, H. Wada, Preparation of Y₂O₃:Er, Yb nanoparticles by laser ablation in liquid, *Appl. Surf. Sci.* 261 (2012) 118–122.
- [48] C.B. Murray, D.J. Norris, M.G. Bawendi, Synthesis and characterization of nearly monodisperse CdE (E = sulfur, selenium, tellurium) semiconductor nanocrystallites, *J. Am. Chem. Soc.* 115 (1993) 8706–8715.
- [49] F.V. Mikulec, M. Kuno, M. Bennati, D.A. Hall, R.G. Griffin, M.G. Bawendi, Organometallic synthesis and spectroscopic characterization of manganese-doped CdSe nanocrystals, *J. Am. Chem. Soc.* 122 (2000) 2532–2540.
- [50] Y. Orikasa, N. Hayashi, S. Muranaka, Effects of oxygen gas pressure on structural, electrical, and thermoelectric properties of (ZnO)₃In₂O₃ thin films deposited by rf magnetron sputtering, *J. Appl. Phys.* 103 (2008) 113703.
- [51] M. Hjjiri, N. Zahmouli, R. Dhahri, S.G. Leonardi, L. El Mir, G. Neri, Doped-ZnO nanoparticles for selective gas sensors, *J. Mater. Sci. Mater. Electron.* 28 (2017) 9667–9674.
- [52] P. Jood, R.J. Mehta, Y. Zhang, G. Peleckis, X. Wang, R.W. Siegel, T. Borca-Tasciuc, S.X. Dou, G. Ramanath, *Nano Lett.* 11 (2011) 4337–4342.
- [53] C. Agashe, O. Kluth, J. Hüpkens, U. Zastrow, B. Rech, Efforts to improve carrier mobility in radio frequency sputtered aluminum doped zinc oxide films, *J. Appl. Phys.* 95 (2004) 1911–1917.
- [54] S. Venkatachalam, Y. Iida, Y. Kanno, Preparation and characterization of Al doped ZnO thin films by PLD, *Superlatt. Microstruct.* 44 (2008) 127–135.
- [55] D. Meljanac, K. Juraić, M. Plodinec, Z. Siketić, D. Gracin, N. Krstulović, K. Salamon, H. Skenderović, Z. Kregar, I. Šrut Rakić, S. Bernstorff, Influence of RF excitation during pulsed laser deposition in oxygen atmosphere on the structural properties and luminescence of nanocrystalline ZnO: Al thin films, *J. Vac. Sci. Technol. A* 34 (2016), 021514-1-10.
- [56] Z. Fan, J.G. Lu, Zinc oxide nanostructures: synthesis and properties, *J. Nanosci. Nanotech.* 5 (2005) 1561–1573.
- [57] C. He, T. Sasaki, H. Usui, Y. Shimizu, N. Koshizaki, Fabrication of ZnO nanoparticles by pulsed laser ablation in aqueous media and pH-dependent particle size: an approach to study the mechanism of enhanced green photoluminescence, *J. Photochem. Photobiol. A* 191 (2007) 66–73.
- [58] C. He, T. Sasaki, Y. Shimizu, N. Koshizaki, Synthesis of ZnO nanoparticles using nanosecond pulsed laser ablation in aqueous media and their self-assembly towards spindle-like ZnO aggregates, *Appl. Surf. Sci.* 254 (2008) 2196–2202.
- [59] S.C. Singh, R. Gopal, Synthesis of colloidal zinc oxide nanoparticles by pulsed laser ablation in aqueous media, *Physica E* 40 (2008) 724–730.
- [60] B.C. Lin, P. Shen, S.Y. Chen, ZnO and ε-Zn(OH)₂ composite nanoparticles by pulsed laser ablation on Zn in water, *J. Phys. Chem. C* 115 (2011) 5003–5010.
- [61] E. Fazio, A. Cacciola, A.M. Mezzasalma, G. Mondio, F. Neri, R. Saija, Modelling of the optical absorption spectra of PLAL prepared ZnO colloids, *J. Quant. Spectrosc. Radiat. Transfer* 124 (2013) 86–93.
- [62] N. Krstulović, P. Umek, K. Salamon, I. Capan, Synthesis of Al-doped ZnO nanoparticles by laser ablation of ZnO:Al₂O₃ target in water, *Mater. Res. Exp.* 4 (2017) 105003.
- [63] N. Krstulović, S. Shannon, R. Stefanuik, C. Fanara, Underwater-laser drilling of aluminum, *Int. J. Adv. Manuf. Technol.* 69 (2013) 1765–1773.
- [64] J.F. Moulder, W.F. Stickle, P.E. Sobol, K.D. Bomben (Eds.), *Handbook of X-Ray Photoelectron Spectroscopy*, Physical Electronics Inc., Eden Prairie, Minnesota, 1995.
- [65] N. Krstulović, S. Milošević, Drilling enhancement by nanosecond–nanosecond collinear dual-pulse laser ablation of titanium in vacuum, *Appl. Surf. Sci.* 256 (2010) 4142–4148.
- [66] H.W. Kang, H. Lee, A.J. Welch, Laser ablation in liquid confinement using a nanosecond laser pulse, *J. Appl. Phys.* 103 (2008) 083101.
- [67] V. Tangwarodomnukun, H.-Y. Chen, Laser ablation of PMMA in air, water, and ethanol environments, *Mater. Manuf. Process.* 30 (2015) 685–691.
- [68] K. Kawabata, Y. Nanai, S. Kimura, T. Okuno, Fabrication of ZnO nanoparticles by laser ablation of sintered ZnO in aqueous solution, *Appl. Phys. A* 107 (2012) 213–220.
- [69] V. Srikanth, D.R. Clarke, On the optical band gap of zinc oxide, *J. Appl. Phys.* 83 (1998) 5447–5451.
- [70] P.L. Washington, H.C. Ong, J.Y. Dai, R.P.H. Chang, Determination of the optical constants of zinc oxide thin films by spectroscopic ellipsometry, *Appl. Phys. Lett.* 72 (1988) 3261–3263.
- [71] J.W. Tomm, B. Ullrich, X.G. Qiu, Y. Segawa, A. Ohtomo, M. Kawasaki, H. Koinuma, Optical and photoelectrical properties of oriented ZnO films, *J. Appl. Phys.* 87 (2000) 1844–1848.
- [72] A.E. Rakhshani, J. Kokaj, J. Mathew, B. Peradeep, Successive chemical solution deposition of ZnO films on flexible steel substrate: structure, photoluminescence and optical transitions, *Appl. Phys. A* 86 (2007) 377–383.
- [73] Kamarulzaman et al., Band gap narrowing and widening of ZnO nanostructures and doped materials, *Nanoscale Res. Lett.* 10 (2015) 346.
- [74] K.K. Kim, D. Kim, S.K. Kim, S.M. Park, J.K. Song, Formation of ZnO nanoparticles by laser ablation in neat water, *Chem. Phys. Lett.* 511 (2011) 116–120.
- [75] H.B. Zeng, W.P. Cai, Y. Li, J.L. Hu, P.S. Liu, Composition/structural evolution and optical properties of ZnO/Zn nanoparticles by laser ablation in liquid media, *J. Phys. Chem B* 109 (2005) 18260–18266.
- [76] C.A. Schaumberg, M. Wollgarten, K. Rademann, Metallic copper colloids by reductive laser ablation of nonmetallic copper precursor suspensions, *J. Phys. Chem. A* 118 (2014) 8329–8337.
- [77] D.S. Zhang, J. Liu, C.H. Liang, Perspective on how laser-ablated particles grow in liquids, *Sci. China-Phys. Mech. Astron.* 60 (2017) 074201.

- [78] Y. Duan, H. Jing, Z. Liu, S. Li, G. Ma, Controlled synthesis and electromagnetic performance of hollow microstructures assembled of tetragonal MnO₂ nanocolumns, *J. Appl. Phys.* 111 (2012) 084109.
- [79] L. Escobar-Alarcón, E. Velarde Granados, D.A. Solís-Casados, O. Olea-Mejía, M. Espinosa-Pesqueira, E. Haro-Poniatowski, Preparation of bismuth-based nanosheets by ultrasound-assisted liquid laser ablation, *Appl. Phys. A* 122 (2016) 433.
- [80] Y.-C. Pu, F. Song, W. Zhang, S. Lindley, S. Adams, J.Z. Zhang, Size-tunable synthesis of hollow gold nanospheres through control of reaction temperature, *Part. Part. Syst. Charact.* 34 (2017) 1600255.
- [81] M. Nafees, W. Liaqut, S. Ali, M.A. Shafique, Synthesis of ZnO/Al:ZnO nanomaterial: structural and band gap variation in ZnO nanomaterial by Al doping, *Appl. Nanosci.* 3 (2013) 49–55.
- [82] H. Liukkonen-Lilja, S. Pippinen, Leaching of aluminium from aluminium dishes and packages, *Food Addit. Contam.* 9 (1992) 213–223.
- [83] R.E. Russo, X. Mao, O.V. Borisov, Laser ablation sampling, *Trends Anal. Chem.* 17 (1998) 461–469.
- [84] C.-A. Tseng, J.-C. Lin, W.-H. Weng, C.-C. Lin, Photoelectron spectroscopy and optical properties of Al-doped ZnO films prepared by sputtering with radio frequency power applied to Al target, *Jpn. J. Appl. Phys.* 52 (2013) 025801.
- [85] H. Zeng, G. Duan, Y. Li, S. Yang, X. Xu, W. Cai, Blue luminescence of ZnO nanoparticles based on non-equilibrium processes: defect origins and emission controls, *Adv. Funct. Mater.* 20 (2010) 561–572.
- [86] K. Vanheusden, C.H. Seager, W.L. Warren, D.R. Tallant, J.A. Voigt, *Appl. Phys. Lett.* 68 (1996) 403–405.
- [87] K. Vanheusden, W.L. Warren, C.H. Seager, D.R. Tallant, J.A. Voigt, B.E. Gnade, Mechanisms behind green photoluminescence in ZnO phosphor powders, *J. Appl. Phys.* 79 (1996) 7983–7990.
- [88] L.B. Kiss, J. Söderlund, G.A. Niklasson, C.G. Granqvist, New approach to the origin of lognormal size distributions of nanoparticles, *Nanotechnology* 10 (1999) 25–28.
- [89] J. Söderlund, L.B. Kiss, G.A. Niklasson, C.G. Granqvist, Lognormal size distributions in particle growth processes without coagulation, *Phys. Rev. Lett.* 80 (1998) 2386–2388.
- [90] F. Mafuné, J.-Y. Kohno, Y. Takeda, T. Kondow, H. Sawabe, Structure and stability of silver nanoparticles in aqueous solution produced by laser ablation, *J. Phys. Chem. B* 104 (2000) 8333–8337.